Simultaneous Tc-99m/I-123 SPECT Brain Imaging using Generalized Spectral Factor Analysis

S Hapdey[1], I Buvat[1], H Benali[1], A Todd-Pokropek[1,2], R Di Paola[1]
[1]U494 INSERM, CHU Pitié-Salpêtrière, Paris, France
[2]Department of Medical Physics, University College London, London, UK

Abstract

In brain SPECT, simultaneous Tc-99m/I-123 acquisitions allow comparison of the distribution of two radiotracers in brain diseases, while avoiding image misregistration issues. However, there is no solution to the cross-talk caused by Tc-99m and I-123 photopeak overlap and by downscatter of I-123 photons into the Tc-99m spectral window and accurate quantification cannot be achieved. We describe a Generalized Spectral Factor Analysis (GSFA) method for solving cross-talk and downscatter problems in simultaneous Tc-99m/I-123 SPECT to improve quantitative accuracy. In GSFA, the spectrum of the photons detected in each pixel is expressed as a linear combination of two photopeaks and K-2 scattered spectra common to all pixels. These basis spectra are estimated using a Principal Component Analysis of all spectra from which a Q-dimensional study space $\mathcal{S}$ is derived. The basis spectra are then identified in $\mathcal{S}$ using priors. Conventional SFA assumes that the number K of basis spectra is equal to the dimension Q of $\mathcal{S}$. We generalized SFA to estimate K factors in a Q-dimensional space, Q>K. Using Monte Carlo simulations of a Tc-99m/I-123 brain phantom, we show that unlike SFA or conventional spectral windows (WIN), GSFA yields accurate quantitative measurements both from the I-123 images (errors <5% against errors between -13% and +14% with SFA and WIN) and from the Tc-99m images with a maximum error less than 4.5%, against errors between 28% and 49% with SFA and WIN.

I. Introduction

In brain SPECT, simultaneous Tc-99m/I-123 SPECT imaging allows comparison of properties and distribution of different receptors or perfusion agents for neuroreceptor mapping or brain disease imaging in an identical physiological state, while avoiding image misregistration issues [1, 2]. These applications would clearly benefit from accurate quantitation to facilitate patient classification.

The major problem with simultaneous dual-isotope SPECT is the problem of cross-talk, that is the detection of photons emitted by a radioisotope in the energy window dedicated to the detection of the other isotope. In Tc-99m/I-123 imaging, cross-talk is caused both by photopeak overlap (close emission energies of 140 and 159 keV respectively) and by photons from I-123 downscattering in the Tc-99m energy window. The magnitude of cross-talk depends on the Tc-99m/I-123 activity ratios but it is admitted that the images are not trustworthy without cross-talk correction [3].

No standard method is currently widely accepted for cross-talk correction. Using specific spectral windows or subtraction methods [4, 5] reduces cross-talk but do not fully remove it. More recently, a spectral factor analysis (SFA) approach has been proposed [6, 7] and promising results were reported for relative quantitation, but the performance of this approach for absolute quantitation remained to be studied.

The purpose of this study was to investigate the quantitative accuracy of Tc-99m/I-123 brain SPECT using Monte Carlo simulations when correcting for cross-talk using a modified SFA approach. As we found that SFA did not yield accurate absolute quantitation, we introduce a generalized spectral factor analysis (GSFA) to achieve accurate absolute quantitation.

II. Generalized Spectral Factor Analysis

This section briefly describes GSFA, derived from Factor Analysis of Medical Image Sequences (FAMIS) in the context of dual-isotope imaging.

In SFA, the energy spectrum of the photons detected in each pixel is modeled as a linear combination of a small number K "basis" spectra to be estimated, namely: isotope 1 (here Tc-99m) photopeak, isotope 2 (here I-123) photopeak and K-2 scatter spectra. This model reads:

$$X_i(e) = \Sigma_{k=1,K}\, a_k(i)\, f_k(e) + \varepsilon_i(e) \qquad (1)$$

where $X_i(e)$ is the number of photons detected in pixel i (i=1,N) at energy e (e=1,P), $a_k(i)$ is the number of photons in pixel i distributed according to the spectrum f_k, $\varepsilon_i(e)$ represents noise or modeling error. For each isotope r, the $a_r(i)$ coefficients associated with photopeak f_r gives the scatter-free image of isotope r, i.e. the image of isotope r corrected for cross-talk. Solving the model consists in estimating the spectra f_k and associated coefficients $a_k(i)$.

Using matrix notation, equation (1) reads:

$$\mathbf{X} = \mathbf{A}\,\mathbf{F}^t + \mathbf{E}, \qquad (2)$$

0-7803-6503-8/01/$10.00 2001 IEEE

where **X**, **A**, **F** and **E** are (N,P), (N,K), (P,K) and (N,P) matrices. The spectra $X_i(e)$ are obtained by acquiring the SPECT data using a multispectral acquisition device, yielding an image series indexed by energy. Using the set of pixel-by-pixel spectra corresponding to this spectral image series, SFA solves equation (2) by using two major steps: first, a correspondence analysis is used to estimate a study space containing **X-E**. Correspondence analysis is adapted to the Poisson nature of the noise in the SPECT projections [8] and yields a Q-dimensional study subspace (typically Q=5) spanned by the Q eigenvectors associated with the largest Q eigenvalues of the covariance matrix decomposed by the correspondence analysis, so that:

$$\mathbf{X} - \mathbf{E} = \mathbf{V}\,\Lambda^{1/2}\,\mathbf{U}^t, \qquad (3)$$

where **V** is the (N,Q) matrix of the eigenimages, **U** is the (P,Q) matrix of the eigenvectors and Λ is the (Q,Q) diagonal matrix of the eigenvalues.

The spectra **F** are then estimated in the study subspace. At this stage, it is assumed in FAMIS (hence in SFA) that *the dimension Q of the study subspace is equal to the number K of spectra to be estimated.* Therefore, estimating **F** in the study subspace is equivalent to finding the coordinates **B** of **F** in the **U** basis:

$$\mathbf{F} = \mathbf{U}\,\mathbf{B}, \qquad (4)$$

B being a (Q,K) matrix. Similarly, estimating **A** is equivalent to finding the coordinates **G** of **A** in the **V** basis with:

$$\mathbf{A} = \mathbf{V}\,\mathbf{G}, \qquad (5)$$

where **G** is a (Q,K) matrix. In addition, one can show that the following relationship between **B** and **G** holds:

$$\mathbf{G}\,\mathbf{B}^t = \Lambda^{1/2}. \qquad (6)$$

F and **A** are estimated using priors such as non-negativity or more complex constraints related to the spectra and associated images by mean of the iterative procedure shown in Figure 1. In this procedure, **G** is estimated from **B** or reciprocally by using equation (6).

Iterations are performed until the difference between two subsequent **F** estimates is negligible.

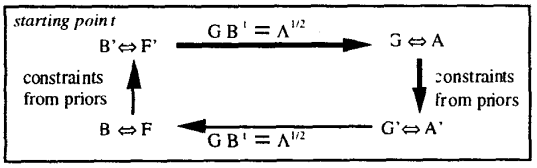

Figure 1: SFA iterative algorithm.

In FAMIS and SFA, the assumption Q=K has always been used. Indeed, using this assumption, B and G are squared matrices of low dimension (K,K) that can be easily inverted during the iterative procedure. However, the validity of this assumption has never really been questioned. We found that this assumption was not always reasonable because the K spectra of interest do not necessarily belong to a K-dimensional study subspace but might belong to a Q-dimensional space with Q>K. In other words, the K spectra having a physical meaning might be only properly described in a study subspace of dimensions Q greater than K. We thus generalized SFA (and FAMIS) to estimate K factors in a Q-dimensional space with Q>K. Such generalization consisted in using a generalized inversion for solving (6) using non squared B and G matrices [9]. In addition, GSFA does not enforce the priors to be strictly verified but allows for relaxation of the constraints associated to these priors using confidence intervals [10].

III. Material and Methods

A. Phantom and simulation

To validate GSFA and characterize the performance of SFA and GSFA for Tc-99m/I-123 brain SPECT, we used Monte Carlo simulations (PHG code [11]) of the anthropomorphic numerical Zubal brain phantom [12]. Activity concentrations of 925 kBq/ml, 740 kBq/ml and 185 kBq/ml Tc-99m were set in the putamen, caudate nuclei and background respectively, while 555 kBq/ml, 925 kBq/ml and 185 kBq/ml I-123 were set in these 3 compartments. The effects of collimator geometric response, scatter and attenuation were modeled. A series of 16 spectral images (from 102 to 178 keV, 4.75 keV sampling) was obtained for each of the 128 simulated projections 128 x 128 (360°, parallel beam geometry, pixel size = 2.2mm, radius of rotation = 25cm). About 15 million photons were detected in the Tc-99m 20% energy window (126-154 keV) and about 15 million photons were also detected in the I-123 20% energy window (145-174 keV).

B. Data analysis

The spectral series corresponding to all projections (one single analysis for all projections of a SPECT acquisition) were processed with SFA and GSFA using the same priors, namely the fact that the Tc-99m and I-123 photopeaks roughly followed known shapes and that the Tc-99m and I-123 first order scatter spectra also roughly followed known energy distributions. The Tc-99m and I-123 photopeak energy distributions were modeled as Gaussian functions with mean = 140 keV and FWHM = 9.8% for Tc-99m and with mean = 159 keV and FWHM = 9.6% for I-123. In addition, the first order scatter spectra for Tc-99m and I-123 were modeled by the convolution of the Klein-Nishina distribution by the gamma camera energy response given by [11]:

$$FWHM_E = y * (Eo)^{1/2} * (E)^{1/2}$$

where y = 9.8% and Eo = 140 keV. Finally, we assumed that the $a_K(i)$ and $f_K(e)$ values were positive as they represent numbers of photons. SFA was performed with K=Q=5, while $GSFA_Q$ was performed using Q between 6 and 16.

In addition to SFA and $GSFA_Q$ processing, we created the projections WIN corresponding to the spectral windows currently recommended for Tc-99m/I-123 imaging [13]: the Tc-99m projections were estimated by considering the events detected in a 130.5-149.5 keV window, while the I-123 projections were estimated using an off-peak 154-178 keV window. The images of Tc-99m primary photons and of I-123 primary photons were also used for reference (REF) as they were not affected by cross-talk.

For each isotope, the REF, WIN, SFA and $GSFA_Q$ projections were reconstructed using the OSEM algorithm (8 subsets, 5 iterations). Before reconstruction, depth-dependent collimator response was compensated for using the frequency-distance principle [14]. Attenuation was modeled in OSEM using the exact attenuation map used for the simulations. A 3D Gaussian post filtering (FWHM = 6 pixels in all directions) was applied to all reconstructed images.

Activity concentrations were measured on the reconstructed Tc-99m and I-123 images in 3D regions of interest (ROIs) corresponding to the putamen (Put), caudate nuclei (Caud) and background (Bgd) drawn on the activity images used for the simulations. Relative quantitation indices were also deduced from these values, namely the putamen to background (Put/Bgd) and caudate nuclei to background (Caud/Bgd) activity ratios in both Tc-99 and I-123 images and the ratio between Tc-99m and I-123 activities in the caudate nuclei, putamen and background ROIs.

IV. Results and Discussion

Figure 2 shows the photopeak and scatter spectra estimated using SFA and $GSFA_{10}$ and the location of the spectral windows used for WIN. This figure and table 1 show that cross-talk in the Tc-99m window was mostly due to scattered photons (15% of the photons detected in this window were Tc-99m scatter, 21.7% were I-123 scatter and only 4.4% were primary I-123). Regarding I-123, 34% of the primary I-123 photons were not detected in the I-123 energy window. Among the photons detected in the I-123 window, 0.7% were from Tc-99m scatter and 12.2% were from I-123 scatter.

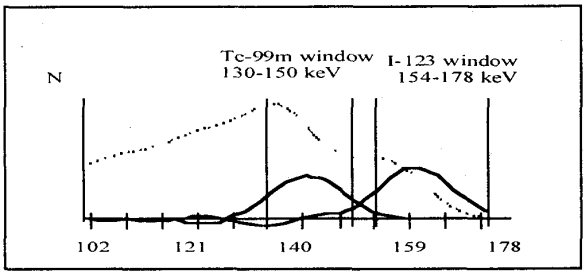

Figure 2a: Spectral windows and spectra estimated using SFA. Dotted line: sum of the 3 scatter spectra.

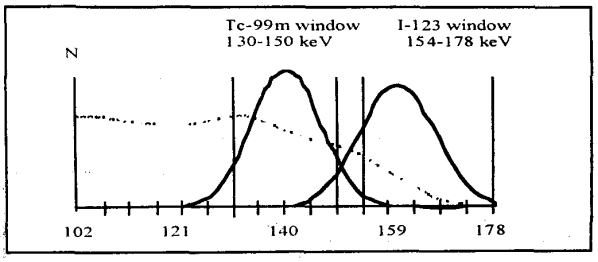

Figure 2b: Spectral windows and spectra estimated using $GSFA_{10}$. Dotted line: sum of the 3 scatter spectra.

This figure and table 1 shows that cross-talk in the Tc-99m window was mostly due to scattered photons (15% of the photons detected in this window were Tc-99m scatter, 21.7% were I-123 scatter and only 4.4% were primary I-123). Regarding I-123, 34% of the primary I-123 photons were not detected in the I-123 energy window. Among the photons detected in the I-123 window, 0.7% were from Tc-99m scatter and 12.2% were from I-123 scatter.

Table 1: Contributions of primary and scattered photons in the Tc-99m and I-123 windows and percentage of primary Tc-99m (resp. I-123) photons outside the Tc-99m (resp. I-123) window.

	Tc-99m window	I-123 window
Primary Tc-99m	58.9 %	0.7 %
Scatter Tc-99m	15 %	0 %
Primary I-123	4.4 %	87.1 %
Scatter I-123	21.7 %	12.2 %
Excluded primary photons	9.2 %	22.5 %

Table 2 gives the number of counts measured in the different ROIs depending on the processing scheme. The percent errors with respect to the activity measured by considering the primary photons only (no cross-talk) are also shown in parenthesis. Because of I-123 downscatter, Tc-99m activity measured from the Tc-99m spectral windows was overestimated by an average of 40±9% over the 3 considered ROIs. The bias strongly depended on the ROI: e.g., activity was overestimated by 33% in the putamen while it was overestimated by 49% in the background, yielding a putamen/background contrast underestimation. Whereas SFA definitely improved quantitation of Tc-99m activity (mean error = 29±4%), a substantial bias preventing from accurate quantitation was still observed. Using $GSFA_Q$, mean errors in Tc-99m activity estimates decreased from 15±1% (Q=6) to 2±2% (Q=16).

Tableau 2: Number of counts in the different ROIs as a function of the processing scheme and quantitative error with respect to the primary photons only (no cross-talk) in parenthesis.

	REF	WIN	SFA	$GSFA_6$	$GSFA_8$	$GSFA_{10}$	$GSFA_{13}$	$GSFA_{16}$
Put Tc-99m	466.5	621 (33.3)	598 (28.2)	530 (13.7)	441 (-5.5)	491 (5.3)	488 (4.6)	486 (4.2)
Caud Tc-99m	426.9	587 (37.6)	553 (26.6)	489 (14.5)	403 (-5.7)	436 (2.2)	435 (1.9)	433 (1.3)
Bgd Tc-99m	281.3	419 (49.2)	377 (34)	326 (15.9)	278 (-1.2)	285 (1.5)	284 (1.1)	283 (0.8)
Put I-123	366.9	324 (-12)	412. (12.5)	359 (-2.1)	304 (-17)	374 (1.9)	373 (1.7)	373 (1.8)
Caud I-123	405.6	352 (-13)	457 (12.8)	406 (0.1)	337 (-17)	400 (-1.2)	401 (-1.2)	401 (-1.1)
Bgd I-123	264.5	237 (-10)	300 (13.6)	257 (-2.7)	220 (-17)	263 (-0.6)	264 (-0.3)	261 (-0.2)

Regarding the I-123 images, spectral windowing yielded a bias varying from -13% to -10% (mean=-11±2%). This bias was relatively small because of a compensation phenomenon: I-123 unscattered photons excluded from the I-123 narrow spectral window (see Figure 1 and Table 1) are partially compensated by scattered I-123 photons included in this spectral window. Using SFA, the bias varied between 12.5% and 13.6% (mean=13±1%). For Q≥10, $GSFA_Q$ gave results very close to those obtained using the primary photons only (mean error was 1±1%), demonstrating an effective cross-talk correction.

For SFA and GSFA, Figure 3 shows how the quantitative errors varied with the dimension Q of the study space. Quantitation was largely biased for Q=5. This is because in this study subspace, low angle scattered photons that had lost little energy could not be distinguished from unscattered photons, due to the limited energy resolution of the gamma camera and despite the priors regarding the shape of first order scatter spectra that were used. Increasing the subspace dimension to 10 improved quantitation accuracy a lot. As soon as the study subspace was large enough to satisfy the priors, the quantitative bias did not change much, suggesting that the GSFA produced stable results from a certain dimension of the study subspace. Indeed, a study subspace with dimensions Q≥10 contained enough information to distinguish low angle scattered photons from primary photons provided appropriate priors regarding the low angle scatter energy distribution were given.

Moreover, the dimension of the study subspace was not the only source of quantitative bias in SFA (Table 3). The priors used for the analysis also affected the results a lot: when using only the photopeak priors in a Q=10 study subspace, large biases were observed with a mean error of 31.9±3.5% in Tc-99m ROIs and 11.4±1.8% in the I-123 ROIs. Consequently, to achieve accurate absolute quantitation using GSFA, both the the priors and the dimension of the study subspace must be properly chosen. Concerning the choice of the priors, a spectral model for first order scatter must be introduced for these photons to be distinguished from primary photons. Otherwise, first order scatter is confounded with

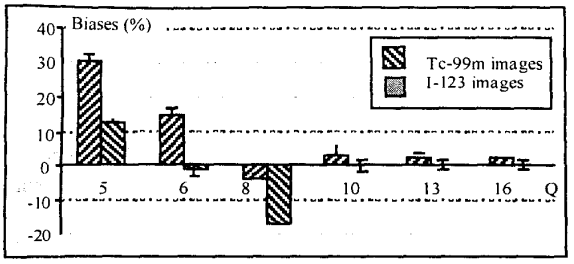

Figure 3: Biases observed in the Tc-99m and I-123 images with $GSFA_Q$ as a function of the dimension Q of the study space.

primary and Tc-99m and I-123 activity are overestimated (Table 3). Regarding the choice of the dimension subspace, our results suggest that as soon as this dimension is large enough for the priors to be met (here Q=10), the exact dimension does not matter much, as the quantitative results remained stable. Looking at the changes of the quantitative estimates with the dimension Q might therefore be enough to determine the appropriate study subspace dimension.

Table 3: Absolute and relative quantitation indices measured with $GSFA_{10}$ processing using photopeak priors only. Quantitative errors with respect to primary photons only (no cross-talk) in parenthesis.

	Put	Caud	Bgd	Put/Bgd	Caud/Bgd
Tc-99 m images	599 (28.5)	555 (30.15)	386 (37.2)	1.55 (-6.4)	1.44 (-5.1)
I-123 images	406 (10.7)	447 (10.2)	299 (13.1)	1.35 (-2.1)	1.49 (-2.6)

Considering relative quantitation (Table 4), the bias affecting striatal/background activity ratios in the Tc-99m or I-123 reconstructed images varied between -11% and -1% with the WIN approach. With SFA and $GSFA_Q$, the bias was almost constant and 2±2% on average, confirming the promising results already observed with SFA for relative quantitation [6]. When estimating Tc-99m/I-123 activity ratios in the different ROIs, the large biases regarding absolute Tc-99m quantitation observed with the WIN approaches resulted in large biases of Tc-99m/I-123 activity ratio estimates, varying from 50% to 67% depending on the ROI. When using SFA for which I-123 absolute quantitation was reasonably accurate (Table 2, average error of 13±1%) but Tc-99m absolute quantitation was significantly biased (Table 2, average error of 29±4%), Tc-99m/I-123 activity ratios were systematically overestimated (mean error of 15.6% over the 3 ROIs). Consistent with the results observed for absolute Tc-99m and I-123 quantitation, accurate Tc-99m/I-123 was achieved with GSFA for Q≥10 (errors <4%).

Table 4: Relative quantitation results as a function of the processing scheme and associated errors with respect to the reference (no cross-talk) in parenthesis. Rows 1-4: striatal/background activity ratios in the Tc-99m and I-123 images. Rows 5-7: Tc-99m/I-123 activity ratios in the putamen, caudate nuclei and background ROIs.

	REF	WIN	SFA	$GSFA_6$	$GSFA_8$	$GSFA_{10}$	$GSFA_{13}$	$GSFA_{16}$
Put/Bgd Tc-99m	1.66	1.48 (-11)	1.59 (-4.3)	1.62 (-1.9)	1.58 (-4.4)	1.71 (3.4)	1.72 (3.4)	1.71 (3.4)
Caud/Bgd Tc-99m	1.52	1.4 (-7.7)	1.47 (-3.3)	1.5 (-1.1)	1.45 (-4.5)	1.53 (0.6)	1.53 (0.7)	1.53 (0.5)
Put/Bgd I-123	1.39	1.37 (-1.5)	1.37 (-0.9)	1.4 (0.7)	1.38 (-0.3)	1.42 (2.1)	1.42 (2.1)	1.41 (2)
Caud/Bgd I-123	1.53	1.49 (-3)	1.52 (-0.7)	1.58 (2.9)	1.53 (0)	1.53 (-0.6)	1.53 (-0.8)	1.52 (0.9)
Put Tc/I	1.27	1.92 (50.8)	1.45 (13.9)	1.47 (16.1)	1.45 (13.9)	1.31 (3.3)	1.31 (2.8)	1.3 (2.3)
Caud Tc/I	1.05	1.66 (58.2)	1.2 (14.9)	1.2 (14.4)	1.19 (13.4)	1.09 (3.4)	1.08 (3.1)	1.08 (2.4)
Bgd Tc/I	1.06	1.77 (66.3)	1.25 (18)	1.27 (19.1)	1.26 (18.7)	1.09 (2.1)	1.08 (1.5)	1.07 (0.9)

V. CONCLUSION

Using Monte Carlo simulations, we found that neither spectral windowing nor SFA provided reliable cross-talk compensation for accurate absolute quantitation in simultaneous Tc-99m/I-123 brain SPECT imaging. Indeed, to achieve accurate absolute quantitation, priors regarding the energy distribution of low angle scatter photons (corresponding to high energy scattered photons) have to be introduced so that these photons can be distinguished from unscattered photons. We showed that Klein-Nishina energy distributions could be used to derive appropriate priors regarding the energy distribution of first order scatter. To properly fit an SFA model including these priors, GSFA was introduced. GSFA allowed us to achieve an almost perfect cross-talk correction, with residual biases in relative and absolute quantitation less than 5%. Further work will include the assessment of GSFA performance for other configurations in which cross-talk correction is needed, for instance in cardiac studies involving Tl-201/Tc-99m imaging. The value of the GSFA approach will also be studied in simultaneous emission/transmission imaging protocols in which cross-talk needs to be dealt with.

VI. REFERENCE

[1] M. D. Devous, J. L. Lowe, and J. P. Payne, "Dual-isotope brain SPECT imaging with technetium and iodine-123: clinical validation using Xenon-133 SPECT," *J. Nucl. Med.*, vol. 33, pp. 1919-1924, 1992.

[2] D. S. O'Leary, M. T. Madsen, R. Hurtig, P. T. Kirchner, K. Rezai, M. Rogers, and N. C. Andreasen, "Dual isotope brain SPECT imaging for monotoring cognitive activation: initial studies in humans," *Nucl. Med. Commun.*, vol. 14, pp. 397-404, 1993.

[3] J. M. Links, "Simultaneous dual-radionuclide imaging: are the images trustworthy?," *Eur. J. Nucl. Med.*, vol. 23, pp. 1289-1291, 1996.

[4] J. E. Juni, R. C. Bernstein, R. A. Ponto, and P. M. Nuechterlein, "Simultaneous dual-tracer brain SPECT with Tc-99m-HMPAO and I-123-iodoamphetamine - method and validation," *J. Nucl. Med.*, vol. 32, pp. 956, 1991.

[5] K. Ogasawara, J. Hashimoto, K. Ogawa, A. Kubo, N. Motomura, H. Hasegawa, and T. Ichihara, "Simultaneous acquisition of iodine-123 emission and technetium-99m transmission data for quantitative brain single-photon emission tomographic imaging.," *Eur. J. Nucl. Med.*, vol. 25, pp. 1537-1544, 1998.

[6] I. Buvat, S. Hapdey, H. Benali, A. Todd-Pokropek, and R. Di Paola, "Spectral factor analysis for multi-isotope imaging in nuclear medicine," *IPMI*, pp. p442-447, 1999.

[7] G. El Fakhri, S. C. Moore, M. F. Kijewski, P. Maksud, and A. Todd-Pokropek, "Monte-Carlo evaluation of quantitation in dual-isotope brain SPECT imaging with Tc-99m and I-123 using Spectral Factor Analysis," *IEEE Trans. Nucl. Sci.*, pp. in press, 2000.

[8] H. Benali, I. Buvat, F. Frouin, J. P. Bazin, and R. Di Paola, "A statistical model for the determination of the optimal metric in Factor Analysis of Medical Image Sequences (FAMIS)," *Phys. Med. Biol.*, vol. 38, pp. 1065-1080, 1993.

[9] F. A. Graybill, "Generalized inverse; conditional inverse," in *Matrices with applications in statistics*, 3 ed: Wadsworth publishing company, 1983, pp. 105-148.

[10] I. Buvat, H. Benali, and R. Di Paola, "Statistical distribution of factors and factor images in factor analysis of medical image sequences," *Phys. Med. Biol.*, vol. 43, pp. 421-434, 1998.

[11] R. L. Harrison, S. D. Vannoy, D. R. Haynor, S. B. Gillispie, M. S. Kaplan, and T. K. Lewellen, "Priliminary experience with the photon history generator module of a public-domain simulation system for emission tomography," *Conf. Rec. Nucl. Sci. Symp.*, vol. 2, pp. 1154-1158, 1993.

[12] I. G. Zubal, C. R. Harrell, and E. Smith, "Computerized 3D segmented human anatomy," *Med. Phys.*, vol. 21, pp. 299-302, 1994.

[13] E. Hindié, D. Mellière, C. Jeanguillaume, L. Perlemuter, F. Chéhadé, and P. Galle, "Parathyroid imaging using simultaneous double-window recording of technetium-99-m-sestamibi and iodine-123," *J. Nucl. Med.*, vol. 39, pp. 1100-1105, 1998.

[14] W. S. Xia, R. M. Lewitt, and P. R. Edholm, "Fourier Correction For Spatially Variant Collimator Blurring in Spect," *IEEE Trans. Med. Imaging*, vol. 14, pp. 100-115, 1995.